PCCP

Accepted Manuscript

ROYAL SOCIETY OF CHEMISTRY

www.rsc.org/pccp

Physical Chemistry Chemical Physics
CREATED USING THE RSC LaTeX PCCP ARTICLE TEMPLATE – SEE www.rsc.org/electronicfiles FOR DETAILS
ARTICLE TYPE
www. rsc.org/xxxxxx | XXXXXXXX

first-principles study of the III-IV-V semiconductor nanosheets†

Amrita Bhattacharya,[*a‡] **Saswata Bhattacharya,**[a‡] **and G. P. Das**[a]

Received Xth XXXXXXXXXX 20XX, Accepted Xth XXXXXXXXX 20XX
First published on the web Xth XXXXXXXXXX 200X
DOI: 10.1039/b000000x

Alloying the III-V and IV-IV sheets, leads to III-IV-V nano-composites, such as the BC_2N sheet, having a lower band gap than their parent III-V counterpart while higher cohesive energies. Unlike the well known BC_2N sheet, the formation energy of the III-IV-V sheets with high Z atomic constituents, is much low suggesting in favour of their experimental realisation. From first-principles hybrid density functional calculations, we report a family of group III-IV-V nano-sheets that have their electronic band gap lying between 0.13 - 1.0 eV, which is ideal for device applications. In particular, we compare the electronic, vibrational, mechanical and thermal properties of a set of III-IV-V sheets with their III-V and IV-IV counterpart. The cohesive energies of these III-IV-V sheets are found to be intermediate of their parent III-V and IV-IV counterparts. Other than the structures reported here, alloying with a different atomic constituents having high-Z difference, lead to highly buckled structures with a plane wise separation of the heavy atoms, causing vibrational instabilities in their bonds.

The major drawback in the device application of graphene[1,2] like group IV-IV planar sheets (e.g. Silicene[3,4]) is the absence of an electronic energy band gap. In contrast, the III-V nanosheets, such as the hexagonal boron nitride (h-BN) sheet[5] and others predicted from first-principles[6], have much wider band gap. Therefore, now-a-days a popular branch for device application of these materials is to engineer the band gap of these sheets[7–9]. In the line of band gap engineering, alloying the III-V and IV-IV sheets together could be potentially of great advantage. Due to the structural analogy of the h-BN sheet with graphene, BC_2N sheets have been widely explored till date[10–15], and BC_2N-films containing mixed phases of both graphene and h-BN domains have also been synthesized[16]. The detailed theoretical analysis of large supercell of the BC_2N sheet, shows a tendency towards phase separation of the BN domain from the C domain[11,14]. However, we have restricted our study to small homogeneous unit cell (where each III-V chain is bonded to another IV-IV chain). Analysis of such small unit cell is important for justifying the structural compatibility and lattice matching of the chosen III, IV and V atoms and therefore may ensure if the given III-V and IV-IV sheets would alloy at all (even in separated phases or domains), or the domains have a tendency of separating away completely from each other.

In this article, we report from the first-principles calculations, the structure, electronic structure, relative stabilities, mechanical, vibrational and thermodynamic properties of a new class of composite III-IV-V planar nanosheets. We have systematically taken into account of all possible combinations of III-V and IV-IV nanosheets exhaustively.

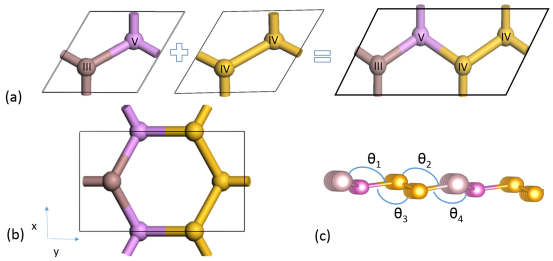

Fig. 1 Crystal structure of III-IV-V planar nanosheets: Fig. (a) shows the top view of the unit cells of the III-V nanosheet and the IV-IV nanosheet, forming the unit cell of the III-IV-V nanosheet, Fig. (b) shows the rectangular equivalent of the hexagonal cell of the III-IV-V nanosheet Fig. (c) shows the dihedral angles between various planes of the III-IV-V sheet.

We have employed density functional theory (DFT)[20,21] calculation using the Vienna ab initio Simulation Program (VASP)[22], which is a pseudo-potential based approach using plane wave basis set. To validate the impact of the chosen exchange-correlation (XC) functional on the stability and electronic structure of these planar nanostructures, we have employed a hierarchical approach including the local density approximation (LDA)[23], the generalized gradient approximation (GGA), i.e.;;, the PBE[24], and the higher-level computations performed with the hybrid functional HSE06[25], which incorporates a fraction of the Hartree-Fock exchange. The en-

† Electronic Supplementary Information (ESI) available: [Table containing the structural properties of III-IV-V nano-sheets, Table for stability analysis of III-IV-V nano-sheets]. See DOI: 10.1039/b000000x/

[a] *Department of Materials Science, Indian Association of the Cultivation of Science, Jadavpur, Kolkata-700032, India*
‡ *Presently at: Fritz-Haber-Institut der Max-Planck-Gesellschaft, Faraday-weg 4-6, D-14195 Berlin, Germany.*
* Corresponding author's email-address: amrita@fhi-berlin.mpg.de [AB]

Table 1 Comparison of the stability, electronic and mechanical properties of the IV-IV and the III-V sheets. The binding energy BE (eV/atom), electronic band gap E_g (eV) are calculated using HSE06 XC functional. Mechanical constants viz. the layer modulus, LM (N/m), the in-plane stiffness IPS (J/m^2) and the Poison's ratio σ are calculated using LDA. SM denotes the semi-metallic electronic states.

System		BE	LM	IPS	σ	E_g	System		BE	LM	IPS	σ	E_g
C	Current	-7.66	217.44	334.85	0.19	SM	BP	Current	-4.09	100.63	135.23	0.28	1.38
	lda[6]			335.00	0.16	SM		lda[6]			135.00	0.28	
	pbe[17]		206.6	342.2	0.17	SM	AlAs	Current	-3.19	46.34	60.02	0.36	2.81
	Expt[18]		209.3	366.4	0.125								
Si	Current	-3.86	45.75	60.40	0.33	SM	AlSb	Current	-2.76	32.20	35.90	0.37	2.08
	lda[6]			62.0	0.30	SM		lda[6]			35.0	0.37	
	pbe[17]		44.5	60.60	0.33	SM	GaP	Current	-3.02	46.94	61.03	0.34	2.92
Ge	Current	-3.19	37.94	48.33	0.35	SM		lda[6]			59.00	0.35	
	lda[6]			48.00	0.33	SM	GaAs	Current	-2.73	35.25	49.28	0.35	2.28
	pbe[17]		29.6	42.70	0.35	SM		lda[6]			48.00	0.35	
Sn	Current	-2.43	24.79	28.35	0.41	SM	GaSb	Current	-2.41	29.28	37.07	0.36	1.37
BN	Current	-6.84	186.24	263.28	0.22	6.28	InAs	Current	-2.45	30.33	34.61	0.42	1.67
	lda[6]			267.00	0.21			lda[6]			33.00	0.43	
	pbe[17]		176.8	275.8	0.22		InSb	Current	-2.23	24.29	27.67	0.42	1.52
	Expt[19]		163.1	258.3	0.22			lda[6]			27.00	0.43	

ergy and atomic force convergences of less than 10^{-4} eV and 0.001 eV/ $\AA$ respectively are set throughout our calculations. To prevent interactions between the adjacent cells a vacuum spacing of 15 $\AA$ is fixed and the pressures on each unit cell is converged up to values less than 0.001 eV/ $\AA^3$. An energy cut off of 600 eV is employed for all the elemental constituents. To optimize the structures (using conjugate gradient minimization), the Brillouin zone is sampled by Monkhorst-Pack method[26]. K-meshes of 16 × 16 × 1 is used to optimize the structures, while a finer (30 × 30 × 1) mesh is chosen for obtaining the electronic density of states (eDOS). To check the accuracy of the quasi-particle gap of few of the test cases, we have also performed G_0W_0[27] on top of the PBE_0[28] (Perdew-Burke-Ernzerhof hybrid) orbitals as reference (namely, G_0W_0@PBE0). The long range dispersion correction is also included.[29]

The phonon frequencies are obtained from the 'Dynamical matrix'[30,31] consisting of the Hessians (containing the second order force constants) constructed via the finite displacement method as implemented in the phonopy code[32] with VASP as the force calculator.

The binding energies (BE) of the sheets are calculated through the following equation,

$$\mathrm{BE}[A_nB_n] = \mathrm{E}[A_nB_n] - n \times \mathrm{E}[A] - n \times \mathrm{E}[B] \qquad (1)$$

where, E[A] and E[B] are the total energies of the A and B single atoms and E[A_n B_n] is total energy of the unit cell with n number of A and B atoms in it.

The formation energies (E_{form}) of the III-IV-V sheets is calculated from their corresponding IV-IV and III-V nanosheets,

$$E_{form} = \mathrm{E}[III-IV-V] - \mathrm{E}[III-V] - \mathrm{E}[IV-IV] \qquad (2)$$

where, E[III-IV-V], E[III-V] and E[IV-IV] are the number scaled total energies of the III-IV-V, III-V and IV-IV nanosheets respectively.

A comparison of the BE (eV/atom) and the electronic band gap, E_g (eV), obtained using different XC functionals are given in the supplementary information (see Table. [SI-2]). For all the planar structures, we find the typical overbinding / underbinding associated with the LDA / PBE functionals respectively in comparison of HSE06 functionals. Except for the sheets with B as one of the constituents, we find that GGA in general underestimates the electronic band gap as compared to LDA by $\sim$ 6-10 %. The electronic and phononic DOS presented in this study are all plotted using the LDA functional, while the correct electronic band gap values are estimated from the HSE06 calculations, which are given in Table. 1.

The in-plane stiffness (IPS) of a planar nanosheet is the measure of its intrinsic strength. The IPS of a planar material is expressed as; IPS = $\frac{1}{A_0}$ ($\frac{\delta^2 E_s}{\delta \varepsilon^2}$); where, E_s = total energy of the strained system and ε is a small strain. The energy of the strained system can be expressed in terms of the strain applied along the x (ε_x) and y (ε_y) direction as,

$$E_s = a_1\varepsilon_x^2 + a_2\varepsilon_y^2 + a_3\varepsilon_x\varepsilon_y \qquad (3)$$

By using a curve fitting method, the coefficient a_1, a_2 and a_3 can be calculated. Once the coefficients are known, the in-plane stiffness, IPS (IPS = $1/A_0(2a_1 - a_3^2/2a_1)$), and the Poisson's ratio, σ ($\sigma = a_3/2a_1$) can be obtained using them. A

Table 2 Comparison of stability, electronic and mechanical properties of the III-IV-V sheets. The binding energy, BE (eV/atom), formation energy E_{form} (eV), electronic band gap, E_g (eV) are calculated using the HSE06 XC functional. Mechanical constants viz. the layer modulus, LM (N/m), the in-plane stiffness, IPS (J/m^2) and the Poison's ratio, σ are calculated by the LDA XC functional.

System	BE	E_{form}	LM	IPS	σ	E_g
BC_2N	-7.01	1.94	197.03	300.50	0.21	2.23
BC_2P	-4.47	3.34	138.00	253.84	0.24	0.37
$AlSi_2As$	-3.40	0.935	41.00	54.12	0.28	0.82
$AlSi_2Sb$	-3.16	1.145	35.25	50.38	0.29	0.73
$AlGe_2Sb$	-2.88	0.786	37.25	40.71	0.30	0.70
$GaSi_2P$	-3.39	0.579	45.95	60.91	0.32	1.06
$GaSi_2As$	-3.22	0.417	41.36	55.34	0.33	0.91
$GaSi_2Sb$	-3.02	0.542	35.20	50.37	0.35	0.80
$GaGe_2P$	-3.05	0.532	42.42	56.41	0.25	0.89
$GaGe_2As$	-2.89	0.478	36.63	48.92	0.32	0.87
$GaGe_2Sb$	-2.73	0.355	32.39	42.59	0.35	0.76
$InSi_2As$	-3.02	0.59	38.92	47.5	0.36	0.57
$InSi_2Sb$	-2.87	0.45	34.81	44.6	0.37	0.13
$InGe_2As$	-2.78	0.52	30.95	40.5	0.38	0.88
$InGe_2Sb$	-2.57	0.37	28.00	37.5	0.38	0.20
$InSn_2As$	-2.41	0.44	27.99	30.28	0.41	0.69
$InSn_2Sb$	-2.38	0.32	24.00	27.44	0.44	0.64

rectangular cell, as shown in Fig. [1(b)], has been employed for this calculations.

In order to cross-check the values of IPS as obtained by above method, we have also adopted an alternate procedure of iterative solution of the 2D Birch-Murnaghan equation of state (BM-E.O.S) as described by Andrew *et. al*[17] to calculate the layer modulus γ ($\gamma = -A\frac{\delta F_l}{\delta A}$) of the sheets, where, F_l ($F_l = -\frac{\delta E}{\delta A}$) is the two dimensional equivalent of bulk pressure and the in-plane strain causes an uniform change in the lattice area of the planar sheet.

A two dimensional equivalent of the BM-E.O.S is given as,

$$E(A) = E_0 + 4A_0\gamma_0\frac{1}{2}\varepsilon^2 + \frac{1}{3}(5-\gamma')\varepsilon^3 + h.o.t. \qquad (4)$$

where, $\varepsilon = \frac{1}{2}(1-\frac{A_0}{A})$ is a small equi-biaxial strain and A_0, γ_0 and γ' are the equilibrium area, the layer modulus and first derivative of the layer modulus respectively. The total energy versus strain data of the hexagonal unit cell, can be fitted with the 2D BM-E.O.S [of equation, Eqn. 4] to solve for A_0, γ_0 and γ' iteratively. The initial guess for E_0 and A_0 corresponds to the minima of the Energy-vs-Strain curve, while the initial guess for γ' is taken as 4.5.

For generating the phonon DOS (phDOS), supercell of 16 × 16 × 1 is employed and q-grids of 20 × 20 × 1 are used.

Once the phDOS is obtained, the thermodynamic free energy, F can be readily obtained by taking the logarithm of the partition function. It should be noted here that we have approximated the free energy PES (potential energy surface) under harmonic approximation;

$$F(T) = \int d\omega g(\omega)[\frac{\hbar\omega}{2} + \mathrm{K}_B T ln(1-e^{(-\hbar\omega/\mathrm{K}_B T)})] \qquad (5)$$

The entropy for the phonons, S is easily calculated by differentiating F with respect to the temperature, from which one can find the heat capacity at constant volume, C_v;

$$\mathrm{C}_v\ (\mathrm{T}) = T\frac{dS}{dT}|_V = -T\frac{\delta^2 F}{\delta T^2}|_V \qquad (6)$$

or,

$$\mathrm{C}_v\ (\mathrm{T}) = \int d\omega g(\omega)\frac{(\hbar\omega)^2}{\mathrm{K}_B T^2}\frac{e^{(\hbar\omega/\mathrm{K}_B T)}}{(e^{(\hbar\omega/\mathrm{K}_B T)}-1)^2} \qquad (7)$$

Finally, the internal energy, U of the phonons could be calculated from the relation, $U = F + TS$;

$$U = \int d\omega g(\omega)[\frac{\hbar\omega}{2} + \frac{\hbar\omega}{e^{(\hbar\omega/\mathrm{K}_B T)}-1}] \qquad (8)$$

The crystal structure of the III-IV-V nano-sheets considered in this study has four atoms per unit cell i.e.; one atom each from group-III and group-V, and two atoms from group-IV, as shown in the Fig. [1(a)]. The stability analysis of various conformers of such small unit cell of the III-IV-V semiconductor nanosheet shows that the structure with one chain of III-V atoms bonded to one chain of IV-IV atoms is the most stable conformation. This energetics is in agreement with the previously reported most stable conformation of the BC_2N sheet[12,13]. However, with increase in cell size ($n \times n$ supercell), the III-V chains have a tendency of separating from the IV-IV chains (i.e.; n III-V chains bonded to n IV-IV chains). This is due to the fact that the IV-IV bonds are stronger than all other bonds in the sheet and therefore, prefer a phase separation. The electronic, vibrational and thermodynamic properties of these sheets would also therefore change if the bigger cell is considered. However, the study of the small unit cell is important for predicting if the III-V sheets will alloy with the IV-IV sheets. Since, it is the best way to check the lattice matching and structural compatibility.

The III-IV-V members having low-Z atomic constituents, such as, the hexagonal BC_2N and BC_2P are found to have completely planar structure while all the other members are found to have a symmetrically puckered planar geometry as shown in Fig. [1(c)]. The dihedral angles (which is also the measure of angle of buckling of these structures), between various planes of these sheets, are found to lie in the range of 10 - 30° (See the supplementary information, Table. SI-1),

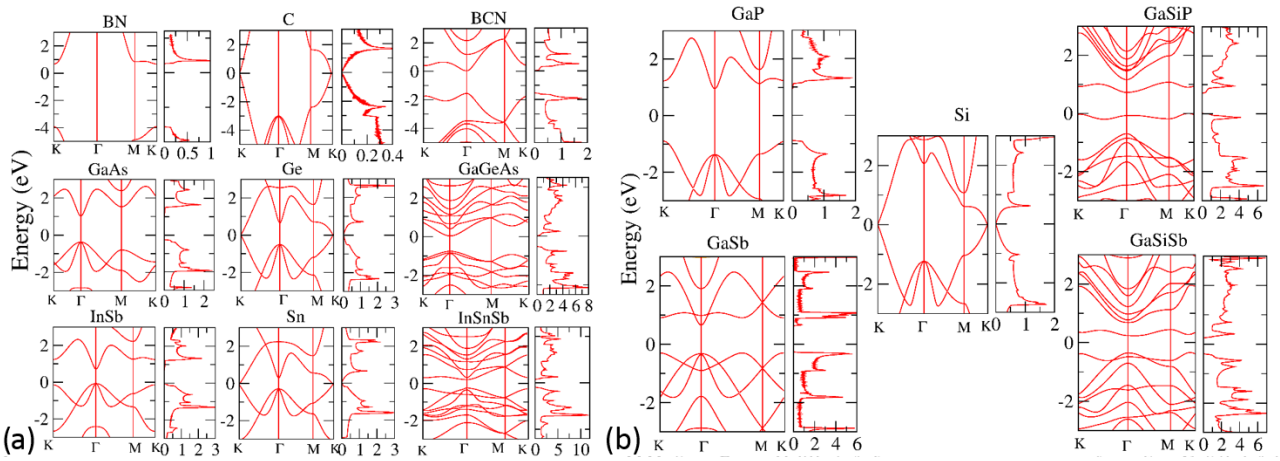

Fig. 2 Electronic band structure and density of states of the representative III-V, IV-IV and III-IV-V planar nanosheets with their atomic constituents (a) from the same period and (b) from the different periods.

thereby, suggesting a low buckling. The low energy structures which do not have any vibrational instabilities in their phonon dispersions (converged with respect to sufficiently large supercell size) are only analysed here.

A comparison of the BEs of the III-IV-V sheets with their III-V and IV-IV counterparts, as calculated by the HSE06 functional, is given in Table. [1]. The binding energies of the IV-IV, the III-V and the III-IV-V sheets follow the general trend:

$$\text{BE [IV-IV]} > \text{BE [III-IV-V]} > \text{BE [III-V]} \qquad (9)$$

The presence of IV-IV bonds in the III-IV-V sheets make them stronger than their III-V counterparts. The BEs of the sheets decrease with the increase of the atomic number (Z) of the constituents, since the III-V and IV-IV bonds get stretched with increasing Z. Since, the C-C bond is the stiffest one, alloying C with III and V atoms having high Z (/ mass/ size) difference leads to a lattice mismatch and leads to a distorted and highly buckled structure with a plane wise separation of the high-Z atoms from the low-Z atoms. Due to the instabilities in their bonds, these structures show negative frequency modes in their vibrational spectra (convergence checked with large supercell size). We observe that amongst the sheets with low-Z difference in their atomic constituents, sheets having Al and N/ Al and P, as their III-V elemental constituents do not alloy with any element from the group-IV, since they also tend to form a highly puckered geometry, showing vibrational instabilities. The comparison of the E_{form} of these III-IV-V sheets (Table. 1) show that the E_{form} decrease with increase in the atomic number of the constituents due to the decrease in the III-V and IV-IV bond strength with increase of atomic number. The low formation energies of these sheets suggest in favour of their realisation through the non-equilibrium routes.

The in-plane stiffness, IPS, layer modulus, LM and the Poisson's ratio, σ of the planar sheets are compared in Table. [1]. The magnitude of IPS of these sheets also decreases with the increase in the atomic number of the constituting atoms i.e.; due to stretching of bonds. The overall trend in the binding energy (Eqn. [9]) is also reflected in the magnitude of their in-plane stiffness and layer modulus. Our calculated values of the in-plane stiffness and Poisson's ratio of III-V and IV-IV sheets are in agreement with the values reported by Sahin *et. al*[6]. The layer modulus of the sheet is also closely related to the IPS[17]. The values of layer modulus of graphene, hexagonal BN-sheet, silicene and germanene are in agreement with the reported values of Andrew *et. al*[17].

The comparison of the electronic band gap, as calculated by the HSE06 functional, of the III-V and III-IV-V sheets is given in Table. [1] and Table. [2] respectively. Unlike to the semimetallic IV-IV sheets, an electronic energy gap (E_g) opens up in the III-IV-V sheets, the E_g values are found to be lower than their III-V counterpart (having much wider band gap). The HSE06 calculations on the BC_2N sheet show that it has the highest band gap of $\sim$ 2.23 eV, while the values of the band gap of all other sheets lie in the range of $\sim$ 0.13-1.0 eV. The $InSi_2Sb$ sheet is estimated to have the lowest band gap of $\sim$ 0.14 eV (see Table. [2]). Most of these III-IV-V sheets are found to have a direct energy band gap at the Γ-point in spite of their IV-IV counterpart being semi-metals with their valence band and conduction band merging at the K-point (see Table. [SI-2]). The G_0W_0@PBE0 calculation of the BN, BP, BC_2N and BC_2P sheets show the quasi-particle gap to be $\sim$ 6.40 eV, 1.48 eV, 2.40 eV and 0.43 eV respectively. These values do not deviate significantly from the results of our HSE-06 calculation as enlisted in Table. [1] and Table. [2]. Therefore, we have relied on the results of the standard hybrid functional

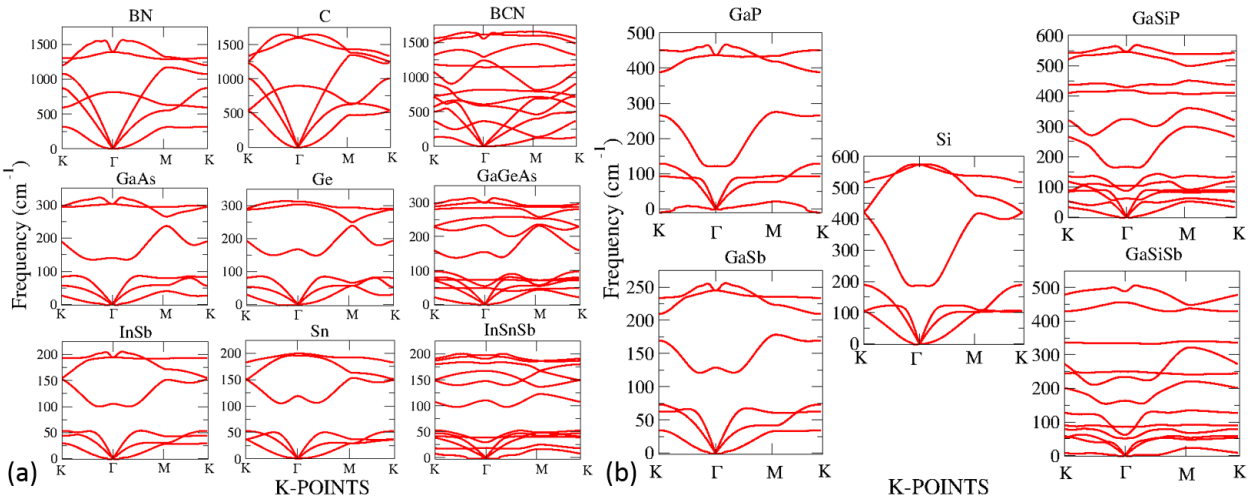

Fig. 3 Phonon dispersions of the representative III-V, IV-IV and III-IV-V planar nanosheets with constituents (a) from the same period and (b) from the different periods.

for rest of these III-IV-V sheets.

The electronic band structure (eBS) and eDOS of few representative members of III-IV-V nanosheet are shown in Fig. [2] with elements belonging to the same period (Fig. [2(a)]), i.e.; with low Z (/atomic mass variation) in its atomic constituents and with elements from different periods i.e.; with high Z (/atomic mass variation) in its constituents (Fig. [2(b)]). High difference in the atomic mass of the constituting atoms leads to dehybridization of the anti-bonding orbital leading to the isolation of electronic bands near the Fermi level as shown in Fig. [2(b)].

The phonon band dispersion (ph-BS) of few selective representatives of III-IV-V nanosheet are shown in Fig. [3]. As the mass of constituting atoms increase, the width of frequency spectrum gets reduced, since heavier atoms have low vibrational amplitude. The III-IV-V nanosheets with atoms belonging to the same period, due to the low mass difference of their atomic constituents, have same spectral width as their III-V and IV-IV counterparts (Fig. [3(a)]). Therefore, their ph-BS are also similar to that of their III-V and IV-IV counterparts i.e.; the acoustic region and the optical region separated by a forbidden gap. However, the spectral width of the III-IV-V sheets having high mass difference in their constituents is determined by vibrational amplitude of the lowest Z constituent. For instance, the GaSb nanosheet has a short spectral width (of 250 cm^{-1}) owing to the heavy atomic mass of the Sb, while the frequency spectrum of silicene sheet is wider (up to 600 cm^{-1}), therefore, the $GaSi_2Sb$ nanosheet has a spectral width of $\sim$ 550 cm^{-1} (close to that of silicene). Since, the III-V and IV-IV parent counterpart of these sheets have different spectral widths and the phonon bands of the III-IV-V sheet are a superposition of them[10], the sheets with high-Z difference in their atomic constituents have their phonon bands spread across the whole spectrum width. So, the acoustic and the optical region in these III-IV-V sheets are not separated from each other (Fig. [3(b)]). We find that most of the IV-IV and III-V sheets have steep acoustical modes (both longitudinal and transverse) with no phonon instabilities as compared to the III-IV-V sheets. The III-IV-V sheets, on the otherhand, have very flat transverse acoustic modes (some time very small instabilities). This may be an outcome of the presence of the heterogeneous III-IV and IV-V bonding at the junctions of III-V and IV-IV chains, which increase the phonon-phonon scattering and therefore, destroy the phonon group velocities i.e.; flatter transverse acoustic modes.

The thermodynamic properties of few selective representatives of the III-V, IV-IV and III-IV-V sheets are compared in Fig. [4]. The F, U, $-TS$ and C_v curves of the III-IV-V nanosheets, follow their parent III-V and IV-IV sheets and are generally found to lie in the middle of the thermodynamic curves of their parent IV-IV and III-V counterparts. Due to low-Z difference in their atomic constituents, the thermodynamic curves of the III-IV-V sheets with their atomic constituents from the same period, are found to be very much similar to each other i.e.; superimposed on one another (Fig. [4(a)]). In sheets with high mass difference in the elemental constituent, the thermodynamic curves are also found to be distinguishable though behaving similar to their parental III-V and IV-IV counterparts (Fig. [4(b)]). From the C_v curves, the Debye temperature (θ_D) of C, BN and BC_2N sheets can be predicted to be much higher (do not reach a saturation in the temperature regime shown) while all the other IV-IV, III-V and III-IV-V sheets have much low θ_D. This behaviour can be explained from their corresponding phonon

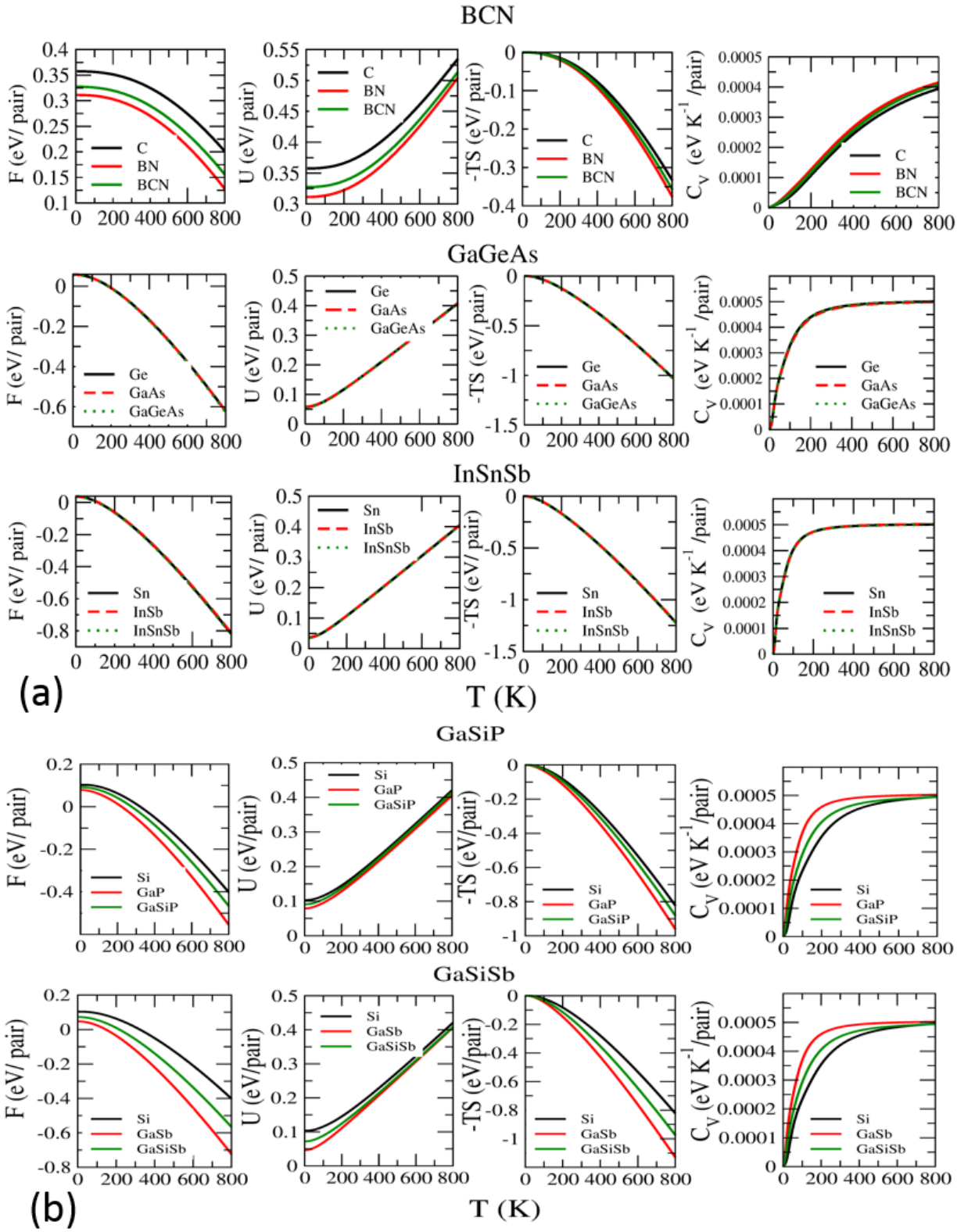

Fig. 4 Variation in the free energy F, internal energy U, $-TS$ (where S is the entropy) and heat capacity C_v of the phonons in the harmonic approximation, of the representative III-V, IV-IV and III-IV-V planar nanosheets with constituents (a) from the same period and (b) from the different periods.

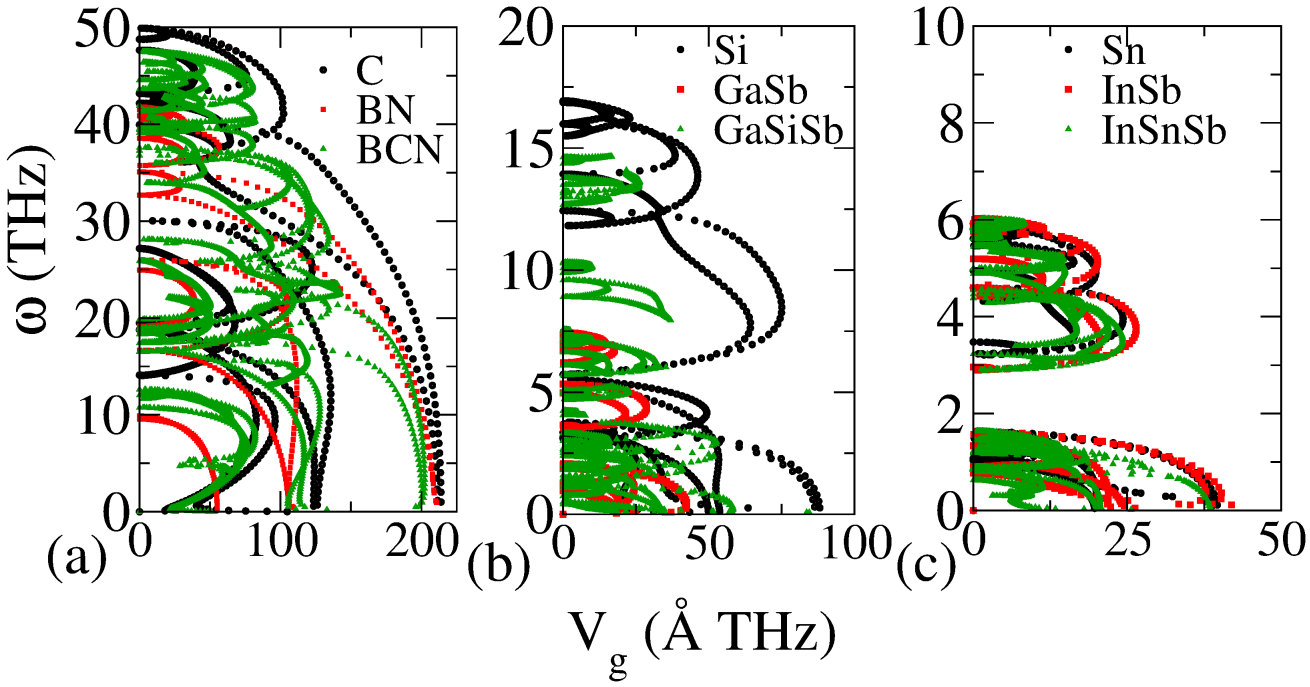

Fig. 5 The phonon group velocities, V_g ($\AA THz$) of various modes of few selective III-V, IV-IV and III-IV-V nanosheets as a function of frequency, ω (THz).

spectrum. The longitudinal acoustic phonon modes of the BN and Graphene (C) sheet have a very steep slope rising to the transverse optical branches. This behaviour is completely absent in the other III-V and IV-IV nanosheets where the acoustic branch have less steep slope (meeting at much less energy at the Brillouin Zone boundary) while the optical branches are well separated by an optical gap. Since, C_v directly depends on the square of ω (see Eqn. [7]), the C_v curves in C, BN and BC_2N also look different that the other IV-IV, III-V and III-IV-V sheets. The steepness of the longitudinal acoustic phonon modes in the BN, C and BC_2N sheets follows from the low mass (m) as well as high bond strength (k) of the constituting atoms in these sheets (since $\theta_D \propto \sqrt{k/m}$). Following this simple argument, the trend of the intrinsic strength (IPS/ LM/ BE) of these sheets can also be verified from their θ_D. The sheets comprising of the first row III, IV, V elements i.e.; B, C, N have the highest IPS/ LM/ BEs followed by that of the sheets comprising of second row and third row elements. The θ_D of the C, BN, BC_2N sheet is also found to be much higher than Ge, GaAs, $GaGe_2As$ sheets followed by the Sn, InSb and $InSn_2Sb$ sheets. This discussion is also applicable for the $GaSi_2P$ sheet and $GaSi_2Sb$ sheets.

The U and F curves of the BC_2N sheet is found to be distinguishable from those of C and BN while their corresponding C_v curves are not. This is also due to the ω dependence of the thermodynamical quantities C_v ($\propto \omega^2$), U and F ($\propto \omega$) as obtained from Eqn. [7], Eqn. [5] and Eqn. [8]. The C_v curve is practically more affected by the variation of ω than the F and U. Since, the phonon dispersion of BN and C sheets are similar and the BC_2N sheet is a combination of these parent modes. The C_v curve of BN, C and BC_2N are found to be indistinguishable (while their U and F curves are found to be distinguishable).

The presence of heterogeneous bonds in the III-IV-V sheets may increase the scattering of the low energy phonons at the junction of the III-V and IV-IV chains and therefore, may lower of the thermal conductivity of these sheet. The thermal conductivity under the Boltzmann transport theory (K= 1/3 C_v $V_g^2\tau$), can be calculated from the specific heat at constant volume C_v, group velocity V_g and phonon lifetime τ. We have plotted the phonon V_g as a function of frequency of few selective III-V, IV-IV and III-IV-V sheets in Fig. [5]. Since, the vibrational spectrum of the BN sheet and graphene do not vary much from each other, the V_g of the phonon modes in the BN sheet, graphene and BC_2N sheet are also not very distinct (Fig. [5(a)]). We observe that for the sheets with low Z difference in its atomic constituent, the V_g of the III-IV-V sheet is lower than its parent IV-IV sheets and III-V sheets (cf. Fig. [5(a)] and Fig. [5(c)]). We also observe that the V_g of the sheets decreases with increase in the atomic mass of the constituents of the sheets. Moreover, the high Z difference in the constituent atoms in the sheet also leads to lowering in

group velocities of the sheets (Fig. [5](b)). The scattering at the junctions may also lead to lowering in the phonon life-times. However, the calculation of the phonon life-times from first-principles involves extremely expensive further computation and therefore will be addressed in our future study. So, in this work, we have not calculated the phonon lifetimes explicitly. But from the comparison of the V_g of the sheets, we can predict the thermal conductivity of these sheets to decrease with increase in Z of the atomic constituents while the electronic band gap of these sheets decreases with increasing Z. Therefore, these sheets might turn out to be good thermoelectric materials[33,34].

In summary, based on our DFT calculations, we report the structure, stability, electronic structure, vibrational and thermodynamic properties of various III-IV-V planar nanosheets. The IV-IV nanosheets are semimetallic, while the III-V sheets have semiconducting band gap. The band gap of these sheets can be tuned by alloying them to form the III-IV-V nanosheets. We have compared the structure, electronic structure, relative stabilities, mechanical, vibrational and thermodynamic properties of these composite III-IV-V planar nanosheets. The range of band gap variation (0.13-1.0 eV) in these III-IV-V sheets may be potentially of great advantage. These III-IV-V sheets have their cohesive energy higher than their III-V counterparts. The puckered geometry and the presence of heterogeneous bonds may result in low thermal conductivity (due to scattering of low energy phonons at the junction of the III-V and IV-IV chains) of these sheets.

References

1 A. K. Geim and K. S. Novoselov, *Nat Mater*, 2007, **6**, 183–191.
2 K. Takeda and K. Shiraishi, *Phys. Rev. B*, 1994, **50**, 14916–14922.
3 P. Vogt, P. De Padova, C. Quaresima, J. Avila, E. Frantzeskakis, M. C. Asensio, A. Resta, B. Ealet and G. Le Lay, *Phys. Rev. Lett.*, 2012, **108**, 155501.
4 A. Bhattacharya, S. Bhattacharya and G. P. Das, *Applied Physics Letters*, 2013, **103**, 123113.
5 C. Jin, F. Lin, K. Suenaga and S. Iijima, *Phys. Rev. Lett.*, 2009, **102**, 195505.
6 H. Şahin, S. Cahangirov, M. Topsakal, E. Bekaroglu, E. Akturk, R. T. Senger and S. Ciraci, *Phys. Rev. B*, 2009, **80**, 155453.
7 D. W. Boukhvalov and M. I. Katsnelson, *Phys. Rev. B*, 2008, **78**, 085413.
8 A. Bhattacharya, S. Bhattacharya and G. P. Das, *Phys. Rev. B*, 2011, **84**, 075454.
9 A. Bhattacharya, S. Bhattacharya and G. P. Das, *Phys. Rev. B*, 2012, **85**, 035415.
10 Y. Miyamoto, M. L. Cohen and S. G. Louie, *Phys. Rev. B*, 1995, **52**, 14971–14975.
11 H. Nozaki and S. Itoh, *Phys. Rev. B*, 1996, **53**, 14161–14170.
12 F. W. Averill, J. R. Morris and V. R. Cooper, *Phys. Rev. B*, 2009, **80**, 195411.
13 S. Jungthawan, S. Limpijumnong and J.-L. Kuo, *Phys. Rev. B*, 2011, **84**, 235424.
14 J. da Rocha Martins and H. Chacham, *ACS Nano*, 2011, **5**, 385–393.
15 S. Bhattacharya, C. Majumder and G. P. Das, *The Journal of Physical Chemistry C*, 2009, **113**, 15783–15787.
16 L. Ci, L. Song, C. Jin, D. Jariwala, D. Wu, Y. Li, Z. F. Wang, K. Storr, L. Balicas, F. Liu and P. M. Ajayan, *Nat Mater*, 2010, **9**, 430–435.
17 R. C. Andrew, R. E. Mapasha, A. M. Ukpong and N. Chetty, *Phys. Rev. B*, 2012, **85**, 125428.
18 A. Bosak, M. Krisch, M. Mohr, J. Maultzsch and C. Thomsen, *Phys. Rev. B*, 2007, **75**, 153408.
19 A. Bosak, J. Serrano, M. Krisch, K. Watanabe, T. Taniguchi and H. Kanda, *Phys. Rev. B*, 2006, **73**, 041402.
20 P. Hohenberg and W. Kohn, *Phys. Rev.*, 1964, **136**, B864–B871.
21 W. Kohn and L. J. Sham, *Phys. Rev.*, 1965, **140**, A1133–A1138.
22 G. Kresse and J. Hafner, *Phys. Rev. B*, 1994, **49**, 14251–14269.
23 J. P. Perdew and Y. Wang, *Phys. Rev. B*, 1992, **45**, 13244.
24 J. P. Perdew, K. Burke and M. Ernzerhof, *Phys. Rev. Lett.*, 1996, **77**, 3865.
25 J. Heyd, G. E. Scuseria and M. Ernzerhof, *J. Chem. Phys*, 2003, **118**, 8207.
26 H. J. Monkhorst and J. D. Pack, *Phys. Rev. B*, 1976, **13**, 5188–5192.
27 L. Hedin, *Phys. Rev.*, 1965, **139**, A796–A823.
28 C. Adamo and V. Barone, *The Journal of Chemical Physics*, 1999, **110**, 6158–6170.
29 A. Tkatchenko and M. Scheffler, *Phys. Rev. Lett.*, 2009, **102**, 073005.
30 K. Kunc and R. M. Martin, *Phys. Rev. Lett.*, 1982, **48**, 406.
31 K. Parlinski, Z. Q. Li and Y. Kawazoe, *Phys. Rev. Lett.*, 1997, **78**, 4063.
32 A. Togo, F. Oba and I. Tanaka, *Phys. rev. B*, 2008, **78**, 134106.
33 K. Yang, Y. Chen, R. D'Agosta, Y. Xie, J. Zhong and A. Rubio, *Phys. Rev. B*, 2012, **86**, 045425.
34 K. Zberecki, M. Wierzbicki, J. Barnaś and R. Swirkowicz, *Phys. Rev. B*, 2013, **88**, 115404.